

Citation for published version:
Song, W, Jiang, Z, Staines, M, Wimbush, S, Badcock, R, Fang, J & Zhang, J 2020, 'Design of a single-phase 6.5 MVA/25 kV superconducting traction transformer for the Chinese Fuxing high-speed train', *International Journal of Electrical Power & Energy Systems*, vol. 119, 105956. https://doi.org/10.1016/j.ijepes.2020.105956

10.1016/j.ijepes.2020.105956

Publication date: 2020

Document Version Peer reviewed version

Link to publication

Publisher Rights CC BY-NC-ND

## **University of Bath**

## **Alternative formats**

If you require this document in an alternative format, please contact: openaccess@bath.ac.uk

**General rights** 

Copyright and moral rights for the publications made accessible in the public portal are retained by the authors and/or other copyright owners and it is a condition of accessing publications that users recognise and abide by the legal requirements associated with these rights.

If you believe that this document breaches copyright please contact us providing details, and we will remove access to the work immediately and investigate your claim.

Download date: 12. Mar. 2023

# Design of a single-phase 6.5 MVA/25 kV superconducting traction transformer for the Chinese Fuxing high-speed train

# Wenjuan Song<sup>1, 2, 3</sup>, Zhenan Jiang<sup>2</sup>, Mike Staines<sup>2</sup>, Rodney A. Badcock<sup>2</sup>, Stuart C. Wimbush<sup>2</sup>, Jin Fang<sup>1</sup>, Jinping Zhang<sup>4</sup>

<sup>1</sup> School of Electrical Engineering, Beijing Jiaotong University, China;

<sup>2</sup> Robinson Research Institute, Victoria University of Wellington, New Zealand;

<sup>3</sup> Department of Electronics & Electrical Engineering, University of Bath, UK;

<sup>4</sup>Bombardier NUG Propulsion System Co., Ltd., China

#### **Abstract**

Traction transformers are critical components of Chinese high-speed-trains. We are currently building a single–phase 6.5 MVA superconducting traction transformer which can achieve targets of less than 3 tons of transformer system weight, better than 99% efficiency, and 43% short-circuit impedance. The proposed transformer consists of four single-phase 25 kV/1.9 kV HTS windings, operating at 65 K, each of which drives a motor. The design incorporates Roebel cable in the LV windings to cope with large current and minimize AC loss. We present 2D FEM AC loss modelling results that identify the critical parameters that contribute to AC loss. We show that the combination of winding length  $\geq 1$  m, high performance Fujikura wires, and flux diverters arranged at the end of HV and LV windings, can restrain AC loss in the HTS windings to under 2 kW. We introduce an open-loop cooling system concept with sub-cooler integrated inside the transformer cryostat that can achieve total system weight under 3 tons assuming 2.5 kW total heat load and 8 hours of continuous running time. A nominal efficiency of 99.5% can be achieved for this total heat load. The entire superconducting transformer system can be readily fit in the space allocated for conventional transformers in the Chinese Fuxing trains.

### Keywords

Traction transformer, High Temperature Superconductors, Efficiency, Transformer weight, AC loss, Cooling system.

#### 1. Introduction

Electrification of transport is a growing trend. Air transportation presents some unique challenges for electrification and these challenges have driven the demand for faster electric rail transport [1]-[2]. The Chinese CRRC Fuxing high speed train is one example of technology being developed, and tested, to be able to operate at 600 km/h [1]. There is a demand to both increase speed, and number of passengers, for these high-speed rail trains. The traction transformer is one of the most critical electrical devices on high-speed-trains, supplying power to four 625 kW traction motors. Fig. 1 shows the layout of the traction transformers currently used in Fuxing high-speed trains. The transformer has two horizontal core legs, each wound with two stacked winding units. Traction transformers must be compact and light-weight, so the current density in the copper wire is much higher than that of utility transformers. As a result the efficiency of the traction transformer may be as low as 94%, much lower than utility transformers, due to high Joule loss in the transformer windings. The windings and core are

enclosed in an oil tank. The heat generated in the transformer tank is removed by circulating oil through a cooling unit with 300 kW cooling power using an oil pump. The specified 43% short circuit impedance of the transformers is high compared to utility transformers, both to limit fault current and to provide reactance for the traction converter power electronics. The transformer tank is 1792 mm long, 1427 mm wide, and 735 mm high tank. The available space for the whole transformer system including the cooling component is 4035 mm long, 2400 mm wide, and 735 mm high. The total weight for the transformer system is approximately 6 tones. Traditional traction transformers - heavy, inefficient, and a fire risk - are prime targets for replacement by high temperature superconducting (HTS) transformers, which can be lighter, more efficient, and a low fire risk.

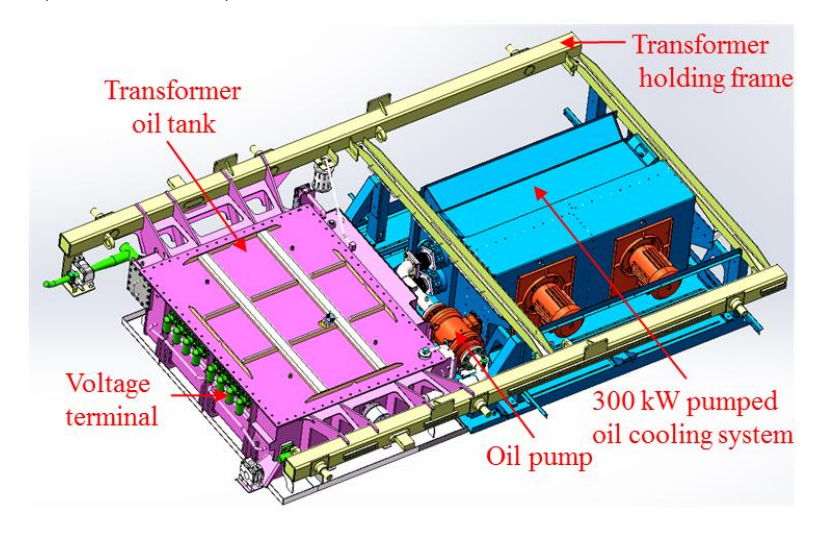


Fig. 1. Layout of traditional 6.5 MVA traction transformer in Fuxing train.

Table 1. List of HTS transformer projects

Year	Country	Organization	Transformer
1997	Switzerland	ABB	3-phase 630 kVA,
			18.72 kV / 0.42 kV
1998	USA	Waukesha Electric Power Company	Single-phase 1 MVA,
			13.8 kV / 6.9 kV
2001	Germany	Siemens	1 MVA, 25 kV / 1.4 kV
2003	Germany	Siemens	Single phase 100 kVA, 5.5 kV/1.1 kV
2004	Japan	Railway Technical Research Institute	4 MVA,
			25 kV / 1.2 kV / 0.44 kV
2005	China	Chinese Academy of Sciences	3-phase 630 kVA,
			10.5 kV / 0.4 kV
2010	New Zealand	Victoria University of Wellington	3-phase 1 MVA,
			11 kV / 0.4 kV
2010	Japan	Nagoya University	3-phase 2MVA, 22 kV/6.6 kV
2013	Japan	Kyushu University	3-phase 2 MVA,
			66 kV / 6.9 kV
2014	Japan	Kyushu University	single-phase 400 kVA, 6.9 kV/2.3 kV
2016	Russia	Russian Scientific R&D Cable Institute	Single-phase 1MVA,
			10 kV / 0.4 kV
2017	China	Shanghai Jiao Tong University	Single-phase 330 kVA, 10.0 kV / 0.231 kV
2019	Switzerland	ABB/KIT	Single phase 577 kVA, 20 kV/1kV

There has been intensive worldwide development in HTS transformers [3] – [19]. Table 1 lists some of these projects. They have shown that controlling AC loss in HTS transformer windings is essential for success. Another important issue is achieving high current in LV windings. Simple vertical stacks

of HTS wires can help increase current carrying capacity of LV winding turns at the expense of large AC loss due to unequal current distribution between the conductors composing the stacks [13], [19], [20]. Parallel connection of multiple LV windings has the same unequal current problem [9]. Two methods have been proposed to solve this problem: coil level transposition (CLT) [15], and using continuously transposed Roebel cables [21] – [25]. A Japanese project [15] has demonstrated 1 kArms for a model HTS winding with 24 parallel conductors using the CLT method, and a NZ group has demonstrated 1390 Arms in LV windings wound with 15/5 (fifteen 5 mm – wide strands) Roebel cable in their 1 MVA 3 phase HTS transformer project [12] – [14].

There have been two examples of HTS traction transformer projects. The Japanese Railway Technical Research Institute and partners demonstrated a three-phase 60 Hz 25 kV/1.2 kV/0.44 kV 4 MVA traction transformer using BSCCO wires operating at 66 K. The transformer had 7 kW AC loss at rated power, and the cryocooler was bigger and heavier than the HTS transformer itself [7], [8], [15]. The other demonstration was a 1 MVA 50 Hz 25 kV/1.4 kV single phase traction transformer manufactured by Siemens using BSCCO Roebel cables for the LV windings. Siemens put their transformer through various electrical and thermal tests [4] - [6]. However, the transformer system was not fully adapted to the actual space available for traction transformers on an electric multiple unit train. In particular, the cooling system was not installed in the transformer space. Moreover, the iron core was cooled down together with the HTS windings so that the heat from hysteretic loss in the core imposed a large load on the cryogenic cooling system. To avoid this the core needs to be located outside the cryostat. The efficiency of the transformer was not stated.

To achieve a high efficiency, light weight, fire-free HTS traction transformer system, an international collaboration project for developing a single phase 50 Hz 25 kV/1.9 kV 6.5 MVA HTS traction transformer was established in 2018. The goal of the project is to demonstrate an HTS transformer which meets the voltage and current specifications in Table 1 and achieve 99% efficiency, less than 3 tons system weight, with 43% short-circuit impedance. The project is led by Beijing Jiaotong University in China, partnered with four other Chinese partners and one non-Chinese organization, the Robinson Research Institute, Victoria University of Wellington.

In this paper, we carried out a feasibility study of a 50 Hz 25 kV/1.9 kV 6.5 MVA HTS traction transformer system operating at 65 K which can be fully integrated in the Chinese fast train system. The analysis reveals that accurate AC loss prediction is crucial: the targets for system weight, as well as efficiency, cannot be met if the AC loss in the transformer windings exceeds 2 kW. Accordingly, we describe our 2D axisymmetric FEM (finite element method) AC loss simulation results in some detail. We also present a concept design for the cooling system, weight analysis for the transformer system, and preliminary layout of the main components of the system. The results demonstrate the feasibility of HTS traction transformers for Chinese high-speed train system, clearly show the advantages over previously demonstrated HTS traction transformer projects by Siemens and Japanese Railway Technical Research Institute. The contents are arranged in the following order. In chapter 2, the

numerical modelling method implementing H formulation is described. In chapter 3, AC loss simulation results are shown. We explored the influence of the transformer winding length (defined in Fig. 2), wire in-field  $I_c$  performance, and flux diverters on AC loss in the transformer windings. In chapter 4, an open-loop cooling system concept in the transformer is described. In chapter 5, total system weight is estimated and arrangement of each system component in standard transformer space for traditional traction transformers is described.

## 2. Numerical method for transformer winding

We chose a basic design for the 50 Hz 25 kV/1.9 kV 6.5 MVA HTS transformer operating at 65 K, where the transformer has four winding units and one leg has two winding units around it as depicted in Fig. 2. Each unit comprises one HV winding, and one LV winding, respectively. All the winding assemblies will be housed in two individual vacuum insulated horizontal cryostats and will be cooled by sub-cooled liquid nitrogen in an open-loop cryocooling system described in chapter 5. An alternative design could place all four winding units on one leg of the core. In this case, we could have only one cryostat which could reduce the weight and cryostat cost. However, AC loss simulation results showed this design has much larger AC loss in the windings and much longer core length which makes the arrangement of the transformer components difficult. Therefore, this option has been excluded. In order to handle a current of 846.0 Arms (1196.4 Apeak) and minimize AC loss in the LV windings, we use continuously transposed 8/5 Roebel cable (eight 5-mm-wide strands). The current in the HV winding is 257 Arms, with the windings for each unit, symmetrically connected in parallel, carrying only 64.3 Arms or 90.9 Apeak current. Therefore, a single 4 mm-wide REBCO superconductor wire will suffice for the HV current. As with previous transformer AC loss modelling [12], [25] we do not consider the iron core in the simulation.

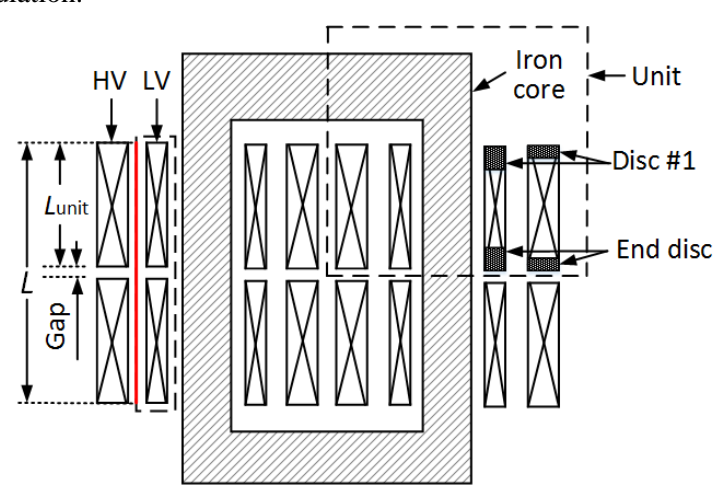


Fig. 2. Schematic of 6.5 MVA traction transformer containing four units each consisting of HV and LV windings. Winding length is defined as *L*.

Numerical calculation for the transformer was carried out in a 2D axisymmetric model, using H formulation [26] – [30]. A homogenization method [30] was implemented in the modelling. The

numerical method is the same as a previous work on the 1-MVA HTS transformer, and more details can be found in the previous publication [25].

Radial and axial magnetic field components  $\mathbf{H} = [H_r, H_z]^T$  are directly solved. Taking into account the symmetry of the transformer windings only a quarter model of a unit was simulated. Schematics of a cross-section of HV and LV winding in one unit only are considered as shown in Fig. 3. Superconducting windings are surrounded by air domain. Current flows in the  $\varphi$  direction.

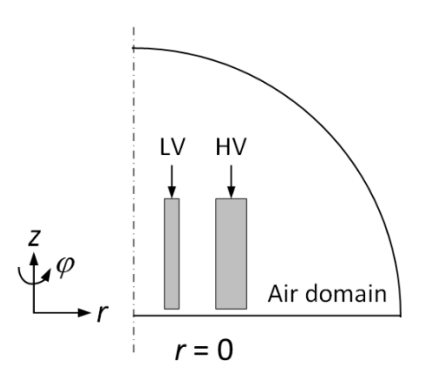


Fig. 3. Schematic of 2D axisymmetric model for 6.5 MVA transformer. (Only a quarter model was simulated.)

The relationship between local electric field  $E_{\varphi}$  and local current density  $J_{\varphi}$  is expressed as,

$$E_{\omega} = \rho J_{\omega} \tag{1}$$

where  $\rho$  is the resistivity of the material. In the air domain,  $\rho$  is treated as a constant; while in the superconducting domain,  $\rho$  is derived from the *E-J* power law,

$$E_{\omega} = E_{\rm c} |J_{\omega}/J_{\rm c}(B)|^{(n-1)} (J_{\omega}/J_{\rm c}(B))$$
(2)

and expressed as

$$\rho = E_{\varphi}/J_{\varphi} = E_{c}|J_{\varphi}/J_{c}(B)|^{(n-1)}(1/J_{c}(B))$$
(3)

where power index n = 25,  $E_c = 10^{-4}$  V/m was used in the work.  $J_c(B)$  is the critical current density dependence on applied magnetic field, which can be derived from the measured  $I_c(B)$  results divided by the cross-section area, S of the superconductor. We adopted a modified Kim model [31] for the  $J_c(B)$  behavior in the calculation,

$$J_c(B) = I_{c0} (1 + (k^2 B_{para}^2 + B_{perp}^2)/B_0^2)^{-\alpha} S^{-1}$$
(4)

where  $I_{c0}$  is self-field critical current,  $B_0$ , k and  $\alpha$  were used as fitting parameters by comparing fitted  $I_c(B)$  curves with measured data under applied magnetic fields. Here,  $B_{perp}$  is the radial magnetic field  $B_r$  and  $B_{para}$  is the axial magnetic field  $B_z$ .

From Ampere's law, we can derive the current density in  $\varphi$  direction along conductor length,

$$J_{\omega} = \partial H_r / \partial z - \partial H_z / \partial r \tag{5}$$

Faraday's law is written as

$$\nabla \times \mathbf{E} = -\partial \mathbf{B}/\partial t = -\mu_0 \mu_r \, \partial \mathbf{H}/\partial t \tag{6}$$

where  $\mu_0$  is vacuum permeability and  $\mu_r$  is relative permeability. Here,  $\mu_r = 1$  everywhere.

Governing equations can be derived from (1) - (6), as

$$\begin{cases}
\mu_{0}\mu_{r}\frac{\partial H_{r}}{\partial t} - \frac{1}{r}\frac{\partial\left(r\rho\left(\frac{\partial H_{r}}{\partial z} - \frac{\partial H_{z}}{\partial r}\right)\right)}{\partial z} = 0 \\
\mu_{0}\mu_{r}\frac{\partial H_{z}}{\partial t} + \frac{1}{r}\frac{\partial\left(r\rho\left(\frac{\partial H_{r}}{\partial z} - \frac{\partial H_{z}}{\partial r}\right)\right)}{\partial r} = 0
\end{cases}$$
(7)

#### 3. Simulation results and discussion

## A. Selection of winding length

In Fig. 2, the HV and LV windings carry opposite current and the axial magnetic field is the strongest in the gap between the HV and LV windings as depicted by the red line in the figure. From Ampere's law, we have:  $\oint H \, dl = NI$ , where H is magnetic field, l is length of the integration loop, NI is the Ampere-turn of the LV winding.

Assuming the magnetic field along the external portion of the loop (dashed line) is negligible, the axial magnetic field component,  $B_z$  can be derived from  $B_z \sim \mu_0 NI/L$  which shows that  $B_z$  can be reduced by increasing the axial winding length, L. Because the continuity of magnetic field, the radical magnetic field component,  $B_r$  near the end of the LV winding should become smaller with increasing winding length L too. The principle should hold true for HV winding. If this is true, the AC loss in transformer windings with longer winding length should be smaller, because the AC loss in the coil windings is dominated by the  $B_r$  components in the end windings [12], [25], [32] – [34].

In order to explore the dependence of AC loss in the transformer windings, AC loss simulation was carried out on four transformer winding designs with different winding length shown in Table 3. The winding lengths are 0.38 m, 0.6 m, 1 m, and 1.5 m, designated as L038, L06, L1, and L15, respectively. More detailed design parameters are given in Table 2. The HV windings comprise stacks of double pancake coils and the LV windings are multi-layer solenoid windings. Each 8/5 Roebel cable turn was simulated as two parallel stacks each with four conductors with the same current in each conductor [35]. Even though the solenoid layer winding is helical, the 3D shape of the winding was simplified and we regarded them as disc windings in our simulation. Therefore, two disc windings in the LV winding are equivalent to one turn of Roebel cable.

Table 2. Specifications of winding design with different winding length

	L038	L06	L1	L15
Winding length $L$ (m)	0.38	0.6	1	1.5
Number of turns in each HV winding disc	38	24	14	9
Number of discs stacked to make the HV winding per unit	42	68	116	174
Number of layers of 8-strand Roebel cable in LV winding	8	5	3	2
Number of turns in one layer in LV winding	15	24	40	60
Number of total turns per unit in HV winding	1596	1632	1624	1566
Number of total turns per unit in LV winding	120	120	120	120
Inner diameter of HV winding (mm)	348	381	437	495
Inner diameter of LV winding (mm)		285	285	285
Axial gap between the two units on each leg of the core (mm)		20	20	20
Short-circuit impedance (%)		43	43	43

To demonstrate the effect of the winding length on AC loss, we modelled the transformer windings with different winding lengths wound with the same wires. We fit (4) to the measured  $I_c(B)$  data of a high-performance Fujikura wire sample (shown later in Fig. 8) to obtain fit parameters  $I_{c0} = 1140$ A/cm at 65 K,  $B_0 = 100$  mT, k = 0.71 and  $\alpha = 0.23$ .

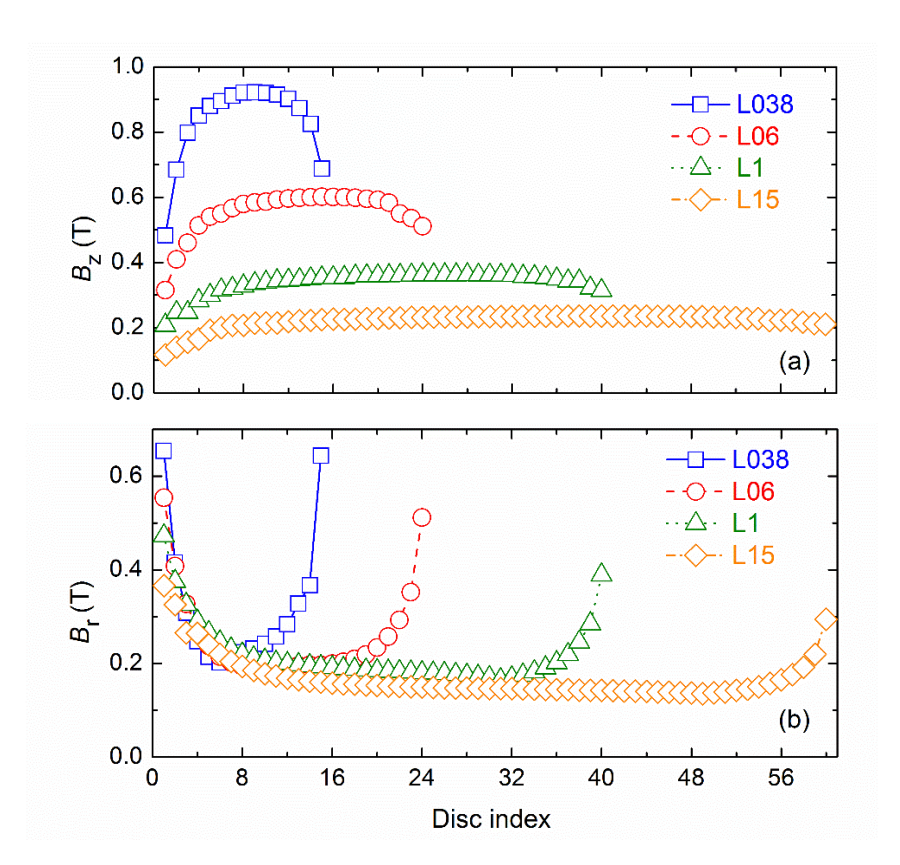


Fig. 4. Magnetic field distribution along inner diameter of LV winding discs for transformers with various winding lengths. a)  $B_z$  component values along the central axial line between the HV and LV. b)  $B_r$  component along the inner diameter of the LV windings.

Fig. 4(a) shows the  $B_z$  component values along the central axial line between the HV and LV windings (see Fig. 2) in L38, L06, L1, and L15 plotted as a function of the turn index of the LV winding.

As shown in the figure,  $B_z$  values were significantly reduced by increasing the winding length. The  $B_z$  values of L38, L06, L1, and L15 are 0.95 T, 0.6 T, 0.35 T, and 0.20 T, respectively, in the central part of the winding unit.

Fig. 4(b) shows the  $B_r$  component along the inner diameter of the LV windings in L38, L06, L1, and L15 transformers. In all LV windings, the  $B_r$  component is small in the central turns.  $B_r$  component in the end turns of the transformers, decreases with increasing the winding length. The asymmetry of the  $B_r$  and  $B_z$  amplitude at the top and bottom turns of the transformer windings results from cancellation of the radial magnetic field components and addition of axial components near the gap between the upper and bottom units.

Fig. 5 shows the calculated AC losses for the transformer, i.e. the summed loss of the four winding units, with various winding lengths. AC loss decreases with increasing winding length. This is consistent with the reduction of the radial magnetic field component in the end part of the transformer windings with winding length. One might argue that large winding length is not preferable, because longer winding length means a longer, heavier iron core. However, shorter windings length have larger AC loss resulting in greater total system weight as discussed in chapter 5. Although the winding with 1.5 m length has lowest AC loss, we select 1 m winding length for the transformer design because a transformer with longer winding is difficult to arrange transversely to the direction of travel, making system integration difficult.

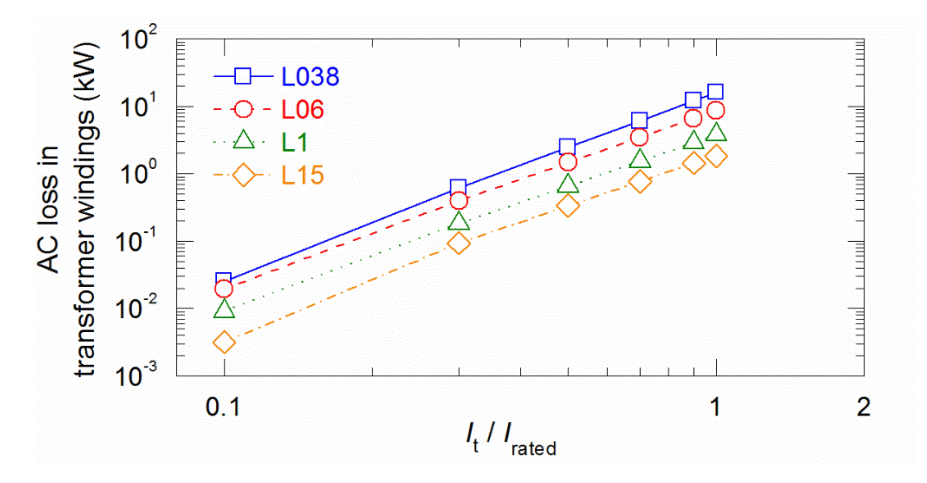


Fig. 5. Calculated AC loss in the transformer with winding lengths of 0.38 m, 0.60 m, 1 m, and 1.5 m, respectively. The winding current is normalized by the rated current of the HV and LV windings.

The AC loss in each disc at rated current in the HV and LV windings for different winding lengths is plotted as a function of disc index in Figs. 6(a) and 6(b), respectively. It should be noted that "disc" in Fig. 6(b) means Roebel disc. In both HV and LV windings, AC loss in the end discs is much bigger than in central discs. The larger AC loss is due to the concentration of the radial magnetic field component at the winding ends, and small AC loss in the central discs is due to cancellation of radial magnetic field in the middle discs [29]. The AC loss in the end part of both HV and LV windings increases significantly with decreasing winding length. AC loss values in the outer end disc are bigger

than the inner end disc for all transformer designs. This is due to the proximity of the upper and lower winding units resulting in cancellation of the radial field at the inner winding ends. In the following figure, more detailed current density distributions for the windings are shown to elucidate the AC loss results.

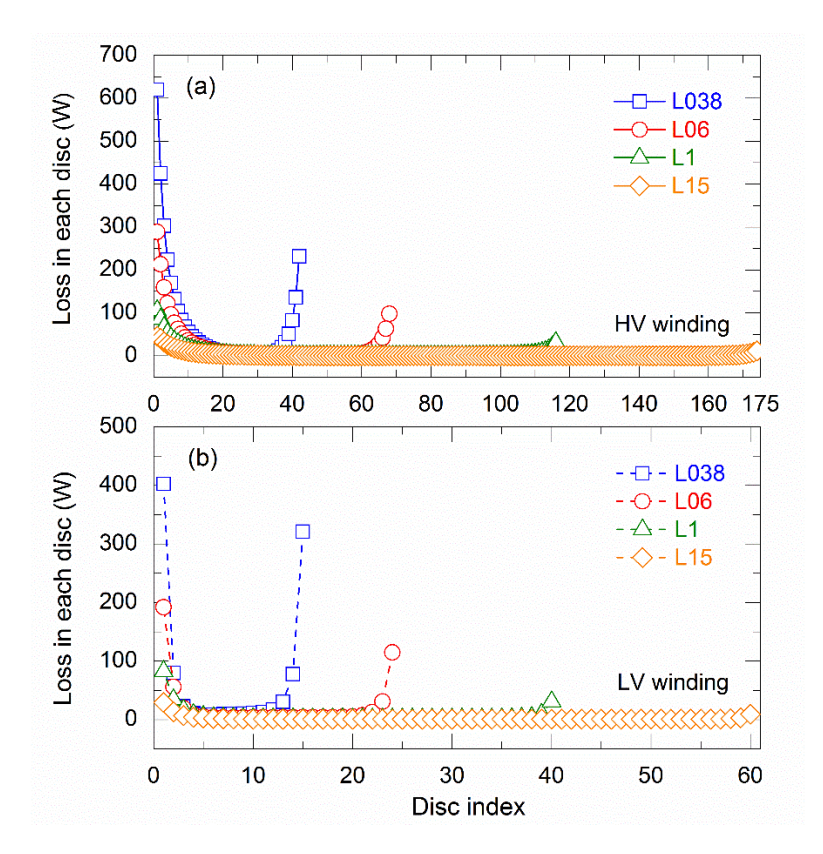


Fig. 6. Loss density distribution in transformer windings with various winding length. a) HV winding. b) LV winding.

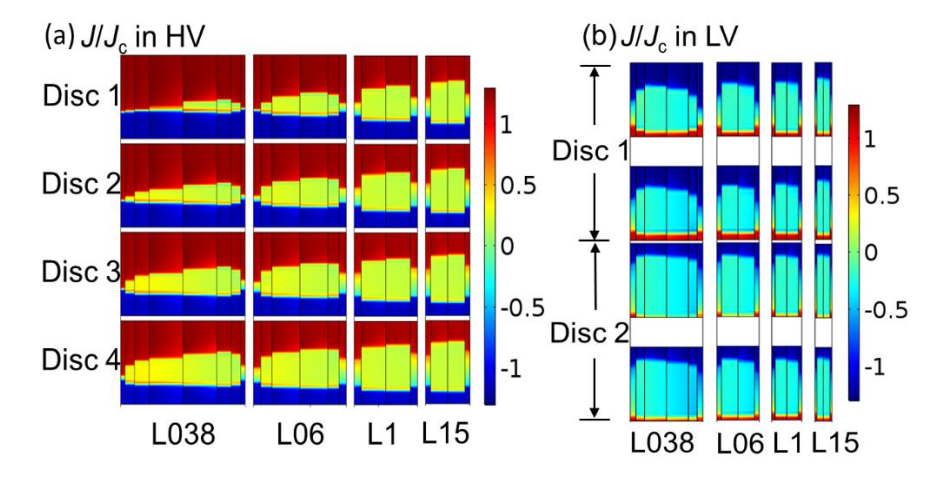


Fig. 7. Comparison of  $J/J_c$  distribution in transformer winding with different winding lengths. a) HV winding. b) LV winding. Disc in b) means Roebel disc.

Fig. 7 shows the  $J/J_c$  distribution and magnetic field distribution of top discs of HV and LV windings with various winding lengths at rated current. In all discs in Fig. 7, there is current flowing in the reverse direction to the coil current in order to shield the radial magnetic field components in the discs [28]. Magnetic field has fully penetrated the superconductors where  $|J/J_c| > 1$ . The region where  $|J/J_c| > 1$  is the biggest in L038 and the least in L15.

## B. Impact of wire $I_c(B)$ performance

AC loss calculations were performed using three different characteristics for wire  $I_c(B)$  at 65 K chosen to study the impact of different aspects of wire performance on the AC loss of the transformer.  $I_c(B)$  for wire #1 was the same data used earlier to select the optimal winding length, measured on a sample of high-quality wire supplied by Fujikura Ltd.  $I_c(B)$  for wire #2 is the same characteristic as wire #1, but scaled down by 20% such that the self-field  $I_c$  at 65 K is reduced from 1140 A/cm to 912 A/cm to reflect the performance of wire available at the time in the quantity required for the transformer windings.  $I_c(B)$  for wire #3 is based on the measured in-field performance of a sample supplied by SuNAM Co. Ltd., but scaled down by 30% to match the self-field  $I_c$  of wire #2. If wire #2 is regarded as a benchmark, wire #1 explores the effect of higher self-field  $I_c$ , while wire #3 explores the effect of greater angular anisotropy in  $I_c(B)$  compared to the relatively isotropic Fujikura wire.

Table 3. Fitting parameters of different wires

	Wire #1	Wire #2	Wire #3
Manufacturer	Fujikura	Fujikura (scaled)	SuNAM (scaled)
I <sub>c0</sub> at 65K (A/cm)	1140	912	915
B <sub>0</sub> (mT)	100	100	102
α	0.23	0.23	0.43
k	0.71	0.71	0.244

Fig. 8 shows the  $I_c(B)$  of the three wires in perpendicular and parallel magnetic fields. Curves fitted using (4) are also plotted, with the fitting parameters used in the AC loss calculations listed in Table 3. The anisotropy of  $I_c(B)$  for wire #3 is apparent in Fig. 8; in 500 mT perpendicular field, its critical field it is 20% higher than wire #2.

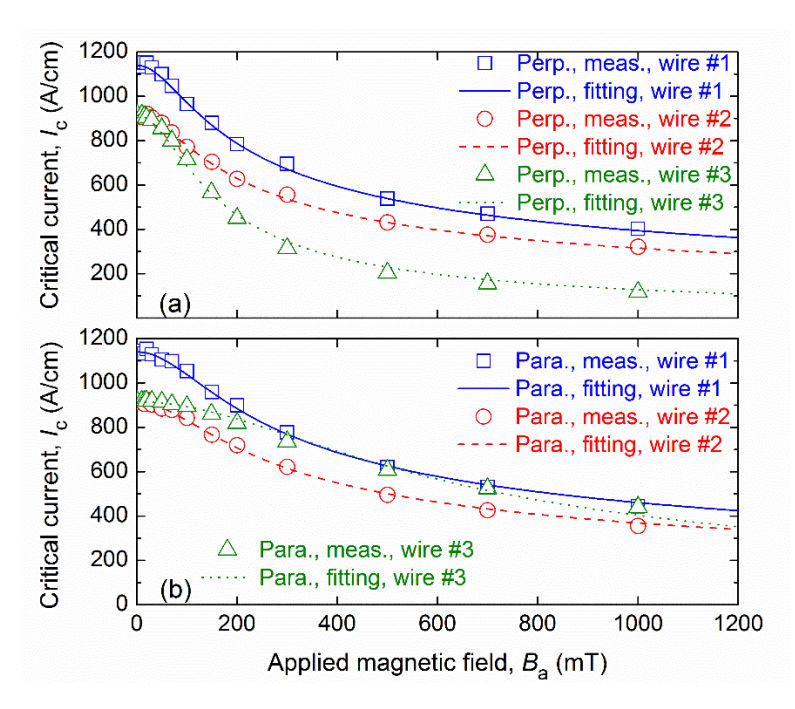


Fig. 8. Field dependence of the critical current at 65 K of different wires (a) in perpendicular magnetic field, and (b) in parallel magnetic field.

Fig. 9 compares the AC loss values in L1\_43% transformers wound with wire #1, wire #2 and wire #3. At rated current, wire #1 has 8% lower AC loss than the benchmark wire #2, while wire #3 has 19% higher loss. The result shows that the AC loss in the windings depends strongly on the critical current in perpendicular magnetic field. Windings made with wire #3 have higher loss than those with wire #2 despite having the same self-field  $I_c$  and higher  $I_c(B)$  in parallel field. In contrast, self-field  $I_c$  has less impact: the AC loss for windings with wire #1 is only 8% less than with wire #2 even though the self-field  $I_c$  is 25% higher.

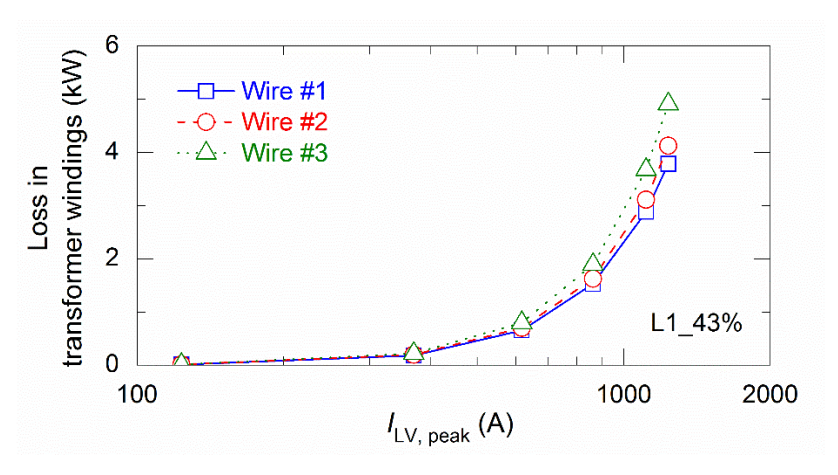


Fig. 9. AC losses in 1 m-long 6.5 MVA transformer winding wound with wires #1, #2, and #3.

Fig. 10 further explains the AC loss behavior shown in Fig. 9 using  $J/J_c$  distribution in the top of the transformer windings wound with wire #1, wire #2, and wire #3 at rated current. The area where  $|J/J_c| > 1$  is the biggest in the transformer wound with wire #3 and the smallest in the transformer wound

with wire #1. We also observe shielding current induced by the radial magnetic field component in the end discs of the HV and LV windings. The simulation results illustrate the importance of  $I_c$  in perpendicular (i.e. radial) field for determining flux penetration in the end turns of the windings, and hence AC loss.

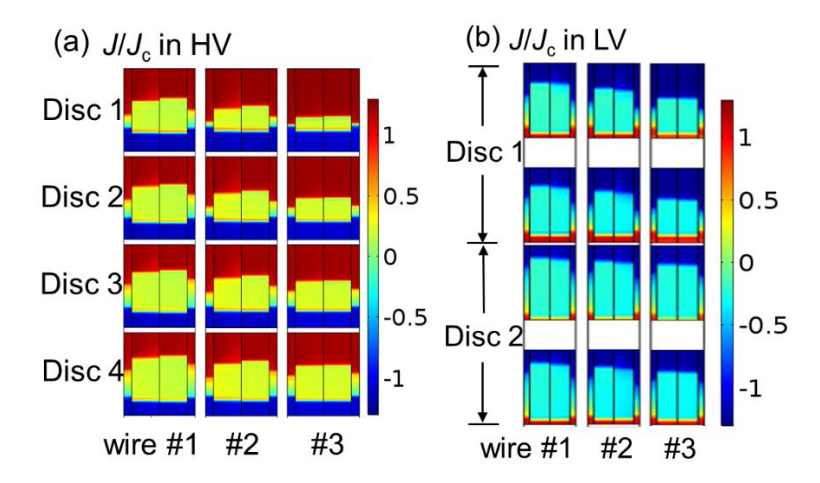


Fig. 10. Comparison of calculated  $J/J_c$  distribution in the outer end turns of the transformer windings using wires with different critical current characteristic. a) HV winding. b) LV winding. Disc in b) means Roebel disc.

### C. Selection of flux diverter

Even best performing L1\_43% transformer design wound with wire #1 has AC loss of 3.79 kW as shown in Fig. 9, much bigger than our target value of 2 kW. Previous reports have shown that AC loss in HTS coil windings can be lowered by arranging flux diverters in the end of the coil windings [37], [38]. In this section we model the effect of adding flux diverters to the L1\_43% transformer design to see if the AC los can be reduced to meet the target.

Fig. 11 shows schematically the arrangement of flux diverters near the outer ends of the HV and LV windings. The cross-section of flux diverters for the HV winding is denoted using  $H_{\text{FD, HV}}$  and  $W_{\text{FD, HV}}$ , and the cross-section of flux diverters for the LV winding is denoted using  $H_{\text{FD, LV}}$ ,  $W_{\text{FD, LV}}$ .  $W_{\text{e}}$  is the distance the flux diverter overhangs both the inner and outer radius of the HV or LV winding. g is the gap between the end of HV/LV windings and the flux diverters. A practical design needs to take into account electrical insulation: the flux diverters and the outer ends of the windings can both be earthed. The inner ends of the top and bottom windings will then be at rated AC voltage, making it problematic to position flux diverters here. In any case, they are not so beneficial between the windings because the radial field component is partially cancelled due to the proximity of the top and bottom windings.

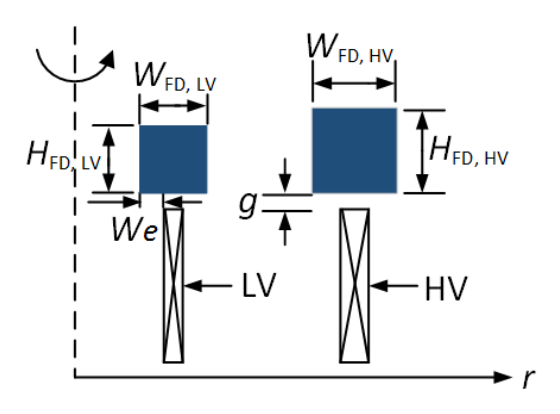


Fig. 11. Schematic of dimensions for flux diverters at end part of windings. For a better vision, the figure was not drawn to scale. (only quarter model)

Table 4. Dimensions of flux diverters

Symbol	FD1	FD2	FD3	FD4	FD5	FD6	FD7
W <sub>e</sub> (mm)	1	5	8	8	8	8	8
g (mm)	0.5	0.5	0.5	0.5	0.5	0.5	0.5
$W_{\mathrm{FD,HV}}(\mathrm{mm})$	6.2	14.2	20.2	20.2	20.2	20.2	20.2
$H_{\mathrm{FD}}$ , HV (mm)	6.2	6.2	6.2	20.2	20.2	20.2	20.2
$W_{\mathrm{FD}}$ , LV (mm)	3.8	11.8	17.8	17.8	17.8	17.8	17.8
$H_{\mathrm{FD,LV}}\left(\mathrm{mm}\right)$	3.8	3.8	3.8	17.8	17.8	17.8	17.8
$\mu_{\rm r}$	100	100	100	50	100	150	$\mu_r(B)$

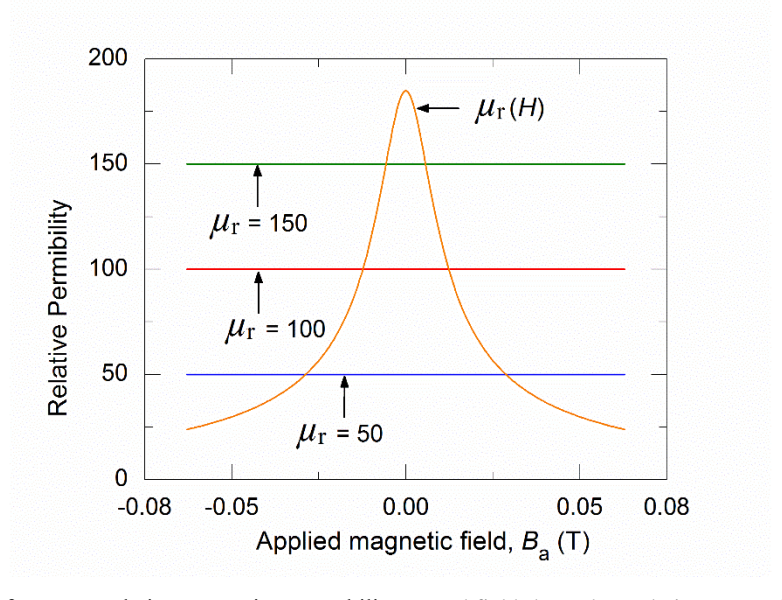


Fig. 12. Comparison of constant relative magnetic permeability,  $\mu_r$  and field-dependent relative magnetic permeability characteristic,  $\mu_r(B)$  of FD7. Here,  $\mu_r(B)$  curve could be fitted as  $\mu_r = 25 + 160e^{-\frac{B^2}{0.000578}}$ .

Seven flux diverters listed in Table 4 were designed to explore their influence on AC loss. FD1, FD2, and FD3 have different  $W_e$  values ranging from 1 mm to 8 mm with a constant  $\mu_r$  value of 100. FD4, FD5, and FD6 have different constant  $\mu_r$  values varying between 50 and 150 with fixed flux diverters dimensions. FD7 has field-dependent  $\mu_r(B)$  using data for sintered NiFe alloy material with a saturation flux density of 1.5 T [36]. Fig. 12 summarizes  $\mu_r$  values used in this study.

Fig. 13 shows the AC loss results as a function of  $W_e$  in L1\_43% transformers using FD1, FD2, and FD3. AC loss in the transformers is significantly decreased using flux diverters: all AC loss in the transformer is substantially decreased. This implies that the flux diverter geometry and positioning plays an important role in AC loss reduction. With FD3, the AC loss in the L1\_43% transformer becomes slightly less than the 2 kW AC loss target for this project.

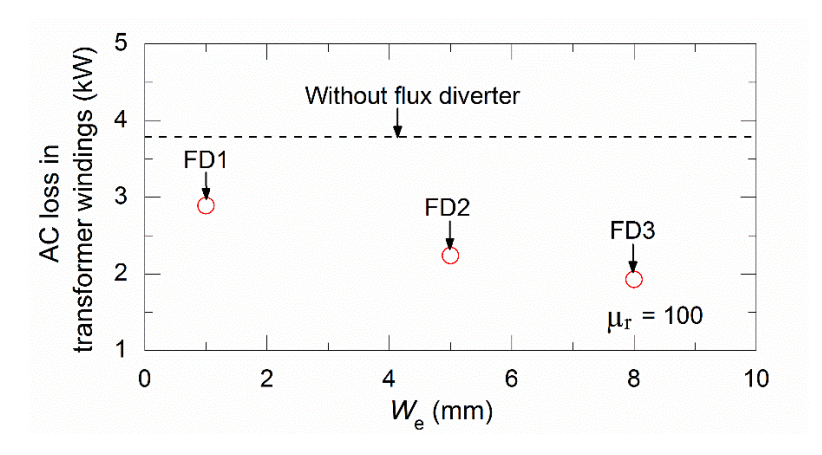


Fig. 13. AC loss in transformer windings with flux diverters installed at the end of windings plotted as a function of We.

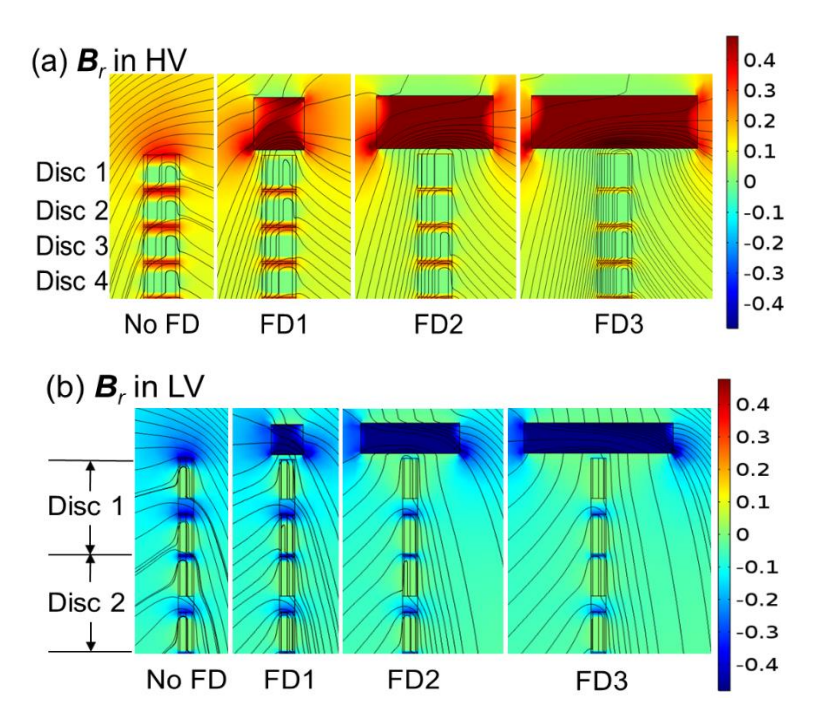


Fig. 14. Distribution of  $B_r$  and magnetic flux in 6.5 MVA transformer designed with different flux diverters (a) HV winding (b) LV winding. Disc in (b) means Roebel disc.

Figs. 14(a) and 13(b) show the  $B_r$  distribution and magnetic stream lines around the top discs of the HV and LV windings of the transformers with and without flux diverters. Both the amplitude of Br and the area filled with large  $B_r$  are the larger in the transformer windings without flux diverters compared with those with flux diverters. Furthermore, the magnetic field is more perpendicular in the discs in the transformer windings without flux diverters. With increasing  $W_e$ ,

magnetic field around the discs becomes more axial (parallel) and the area filled with high amplitude  $B_{\rm r}$  decreases. On the other hand, we can see more concentration of magnetic field inside the flux diverters with increasing  $W_{\rm e}$ .

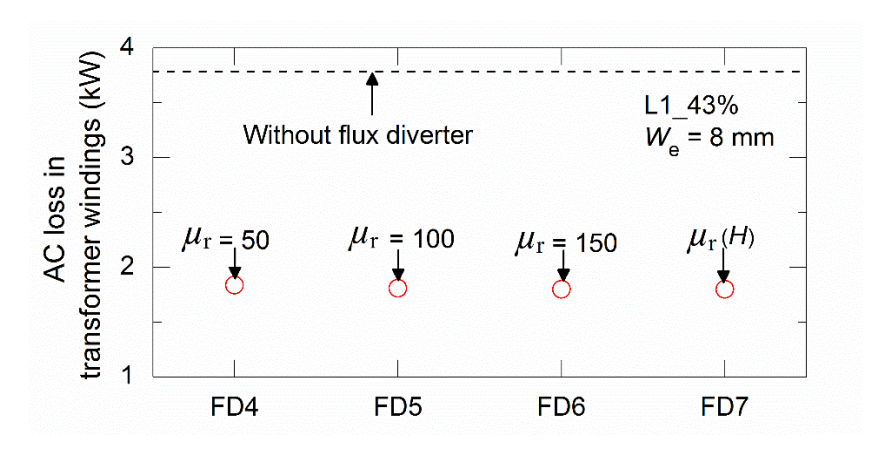


Fig. 15. Comparison of AC loss in transformer windings when installed with flux diverters with different relative permeability.

In Fig. 15, AC loss values for L1\_43% transformers using flux diverters with various  $\mu_r$  values at rated current are compared. The difference in the AC loss values using the flux diverters is negligible which shows that the AC loss in the transformers is not sensitive to  $\mu_r$  values. It is worth noting that that flux diverters have their own hysteresis and eddy current loss. More work needs to be done to find more efficient shapes for the flux diverters to optimize the trade-off between AC loss reduction and hysteretic and eddy current loss in the diverters.

## 4. Concept design of cooling system

The basic specification for the cooling system is for 2.5 kW of cooling power at 65 - 67 K (2.0 kW of AC loss and 0.5 kW current lead and cryostat heat leak). Our plan is to have two epoxy fiber glass composite cryostats, one for each pair of windings units on each leg of the transformer core. Construction of a single cryostat to cool both legs of the transformer might be more thermally efficient but is seen as a high-risk technical challenge.

A fundamental decision for cooling system design is the choice between a closed-loop cooling system using an on-board cryocooler and an open-loop system using pumped cooling from an on-board liquid nitrogen storage tank. The closed-loop system is seen as attractive because it would avoid the need for liquid nitrogen filling facilities at rail terminuses. On the other hand, cryocoolers with the required cooling power are expensive and require more maintenance compared to a storage vessel and vacuum pumps. In any case, there are at present no suitable cryocoolers commercially available that can fit in the limited vertical space available, so the choice has been made to use an open-loop system. In terms of cooling power and operating temperature the requirements for the traction transformer are similar to those for the Ampacity cable cooling system [39]. That system included a sub-cooler and

liquid nitrogen circulation pump. For the traction transformer, we need to cool a compact winding rather than a long cable. We can therefore avoid the weight and complexity of a separate sub-cooler and circulation pumps by bringing the sub-cooler inside the cryostat as shown in Fig. 16, as was done for a recent fault current limiting transformer demonstration [40]. Natural convection is used to transfer heat from the windings to the sub-cooler/heat exchanger.

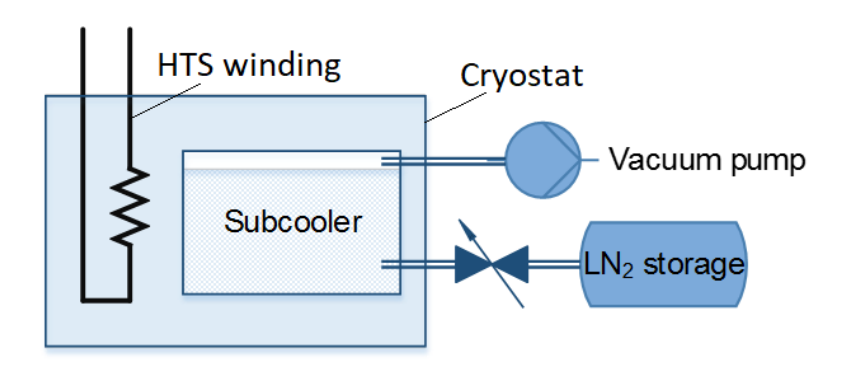


Fig. 16. Schematic of proposed open-loop cooling system using a subcooler / heat exchanger immersed in the sub-cooled liquid nitrogen in each cryostat.

### 5. Estimation of total weight and system component arrangement

The target weight for the HTS transformer system is 3 tons, about half the weight of the conventional transformer system. The system weight is the sum of a fixed component for the transformer and cryostats, a second component that depends on the cooling power required, and a third component that depends on the product of cooling power and running time, i.e. the amount of stored liquid nitrogen to be carried on-board.

$$M_{total} = M_{fixed} + P_{cooling} \left( \frac{\Delta M_{pumps}}{\Delta P} + t_{run} (1 + \alpha) \frac{\Delta M_{LN2}}{\Delta P \Delta t} \right)$$
(9)

The pump mass dependence on cooling power  $(\Delta M_{\text{pumps}})/\Delta P$  is estimated to be 92 kg/kW based on specifications for suitable claw pumps. Assuming storage dewar pressure of 3 bars, the rate of liquid nitrogen consumption per unit cooling power at 65 K  $(\Delta M_{\text{LN2}})/\Delta P\Delta t$  is estimated to be 20.5 kg/kWh from standard specific entropy values. The running time of the transformer cooling system is  $t_{\text{run}}$ , assumed to be in the range 4 to 8 hours. The ratio of the mass of the empty storage vessel to that of its contents is given by  $\alpha$  and can be estimated from  $M_{\text{dewar}} = 400V^{2/3}$ , consistent with manufacturers' specifications, where the liquid nitrogen volume V is in m³, and mass in kg.

Table 5 lists the details of the iron core design for the HTS traction transformer. Table 6 shows an estimate of the weight of the system and its component parts for required cooling power of 2.5 and 5 kW and for running times of 5 and 8 hours. At 2.5 kW cooling power the total system weighs under 3000 kg even for 8 hours running time. At 5 kW cooling power the weight exceeds the target even for the shorter running time. At 8 hours running time the 5 kW system is almost 800 kg heavier than the system with 2.5 kW cooling power. These estimates underline the importance of minimizing AC loss to keep within system weight constraints. If we assume a cooling penalty of 12.65 kW input power per

kW of cooling calculated [34] for liquid nitrogen supplied by a large air separation unit, including energy expended in transport, we estimate the efficiency of the traction transformer to be 99.5%. If we assume an efficient on-board cryocooler with cooling penalty of 16 (Stirling Cryogenics SPC-4), the efficiency of the transformer will be somewhat lower at 99.3%.

Table 5. Iro core dimension

Core extension length (mm)	1720
Core diameter (mm)	225
Core arms center-to-center (mm)	516
Core window height (mm)	1270
Core window width (mm)	291
Core extension width (mm)	741

Table 6. Estimation of system weight

Running time (hours)	5	5	8	8
Cooling power (kW)	2.5	5	2.5	5
LN storage vessel (kg)	186	296	255	404
LN in storage (kg)	256	513	410	820
Pumps (kg)	230	460	230	460
Cryostats (kg)	171	171	171	171
LN in cryostats (kg)	452	452	452	452
Wire, formers, etc (kg)	96	96	96	96
Core (kg)	1223	1223	1223	1223
Total for system (kg)	2622	3220	2847	3639

Fig. 17 shows a possible arrangement of system components in the  $4.036 \text{ m} \times 2.4 \text{ m} \times 0.735 \text{ m}$  space for conventional traction transformers. If we constrain core length to 1.8 m, cryostat height to 0.7 m, cryostat length to 1.2 m, cryostat width to 1.4 m, and pump length to 1.0 m, it is possible to arrange all the transformer components in the available space.

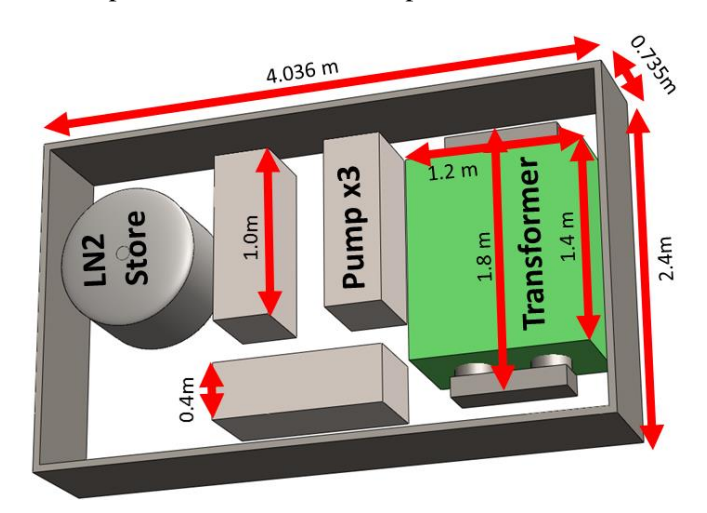


Fig. 17. Suggested arrangement of transformer components in the 4.036 m  $\times$  2.4 m  $\times$  0.735 m standard transformer space.

#### 6. Conclusions

An HTS traction transformer project for Chinese Fuxing high-speed trains has been running since 2018. Our target within this project is to develop a low fire-hazard HTS transformer with 99% efficiency, less than 3 tons system weight, and 43% short-circuit impedance.

AC loss in HTS traction transformer windings decreases with increasing the winding length of a winding unit.

AC loss in transformer windings depends strongly on the critical current in perpendicular magnetic field, while depends less on self-field critical current values.

Flux diverters arranged in the end of the HTS windings substantially reduce perpendicular magnetic field component in the end windings, and significantly reduce AC loss values in HTS traction transformers.

With the combination of 1 m transformer winding length, high performance Fujikura wires, and flux diverters arranged at the outer end of HV and LV windings, we could restrain AC loss in the HTS windings within 2 kW.

An open-loop cooling system design with sub-cooler integrated within the transformer cryostats can achieve total system weight within 3 tons assuming 2.5 kW total heat load for HTS windings and 8 hours of continuous running time.

An efficiency of 99.5% can be achieved assuming a total heat load of 2.5 kW and using the cooling penalty for liquid nitrogen supplied from a large air separation unit. All transformer system components can be integrated in the standard space for conventional transformers in Chinese Fuxing high-speed trains.

In comparison to the Japanese 4 MVA HTS traction transformer having too great AC loss and hence too heavy cooling system and the Siemens 1 MVA traction transformer which failed to demonstrate integrated cooling system in the traction transformer space. Our 6.5 MVA transformer design shows significant advantages in system weight, efficiency, and system integration for the allocated space for traditional transformers. Our work for first time showed the feasibility of HTS technology and potential in rapidly expanding Chinese high-speed Fuxing train system.

## Acknowledgement

This work was supported by Ministry of Science and Technology on National Key Research and Development Program of China under Grant No. 2016YFE0201200.

## Appendix: Main specifications of the Fuxing train traction transformer

Table A lists the main speficiations of the conventional traction transformer.

Table A. Main specifications of the Fuxing train traction transformer

	HV winding	LV winding	
Frequency (Hz)	50		
Rated capacity (kVA)	6433	4 × 1608	
Rated voltage (V)	25000	4 × 1900	
Rated current (A)	257	4 × 846	
Short circuit impedance (%)	43		
Efficiency (%)	95		
Weight (kg)	5920		

#### References

- [1] https://www.weforum.org/agenda/2019/06/china-floating-train-faster-than-air-travel/
- [2] Y. P. Chang, "Optimal harmonic filters design of the Taiwan high speed rail traction system of distributer generation system with specially connected transformers", *International Journal of Electrical Power & Energy Systems*, vol. 62, pp. 80-89, 2014.
- [3] H. Zueger, "630 kVA high temperature superconducting transformer," Cryogenics, vol. 38, no. 11, pp. 1169-1172, 1998.
- [4] S. Schwenerly, B. McConnel, J. Demko, et al., "Performance of a 1-MVA HTS demonstration transformer," *IEEE Transaction on Applied Superconductivity*, vol. 9, no. 2, pp. 680-684, Jun. 1999.
- [5] M. Leghissa, B. Gromoll, J. Rieger, et al., "Development and application of superconducting transformers," *Physica C*, vol. 372, pp. 1688-1693, 2002.
- [6] R. Schlosser, H. Schmidt, M. Leghissa, et al., "Development of high-temperature superconducting transformers for railway applications," *IEEE Transaction on Applied Superconductivity*, vol. 13, no. 2, pp. 2325-2330, Jun. 2003.
- [7] M. Meinert, M. Leghissa, R. Schlosser, et al., "System test of a 1-MVA-HTS-transformer connected to a converter-fed drive for rail vehicles," *IEEE Transaction on Applied Superconductivity*, vol. 13, no. 2, pp. 2348-2351, 2003.
- [8] H. Kamijo, H. Hata, H. Fujimoto, et al., "Fabrication of inner secondary winding of high-Tc superconducting traction transformer for railway rolling stock," *IEEE Transaction on Applied Superconductivity*, vol. 15, no. 2, pp. 1875-1878, Jun. 2005.
- [9] H. Kamijo, H. Hata, Y. Fukumoto, et al., "Development of low AC loss windings for superconducting traction transformer," *Journal of Physics: Conference Series*, vol. 234, no. 3, Art. no. 032027, 2010.
- [10] Y. Wang, X. Zhao, J. Han, et al., "Development of a 630 kVA three-phase HTS transformer with amorphous alloy cores," *IEEE Transaction on Applied Superconductivity*, vol.17, no. 2, pp. 2051-2054, Jun. 2007.
- [11] M. Iwakuma, K. Sakaki, A. Tomioka, et al., "Development of a 3  $\phi$  -66/6.9 kV-2 MVA REBCO superconducting transformer," *IEEE Transaction on Applied Superconductivity*, vol. 25, no. 3, Art. no. 5500206, 2015.
- [12] N. Glasson, M. Staines, Z. Jiang, and N. Allpress, "Verification testing for a 1 MVA 3-phase demonstration transformer using 2G-HTS Roebel cable," *IEEE Transaction on Applied Superconductivity*, vol. 23, no. 3, Art. no. 5500206, Jun. 2013.
- [13] E. Pardo, M. Staines, Z. Jiang, and N. Glasson, "Ac loss modelling and measurement of superconducting transformers with coated-conductor Roebel-cable in low-voltage winding," *Superconductor Science and Technology*, vol. 28, no. 11, Art. no. 114008, Oct. 2015.
- [14] M. P. Staines, Z. Jiang, N. Glasson, et al., "High-temperature superconducting (HTS) transformers for power grid applications" *Superconductors in the power grid: Materials and applications*, Ch 12, Woodhead Publishing series in Energy, C. Rey, Ed. Elsevier, 2015.
- [15] M. Iwakuma, H. Hayashi, H. Okamoto, et al., "Development of REBCO superconducting power transformers in Japan," *Physica C*, vol. 469, no. 15, pp. 1726-1732, Jun. 2009.

- [16] M. Kotari, H. Kojima, N. Hayakawa, F. Endo, and H. Okubo. (2010). "Development of 2 MVA class superconducting fault current limiting transformer (SFCLT) with YBCO coated conductors," Journal of Physics: Conference Series, vol. 234, no. 3, Art. no. 032070, 2010.
- [17] Y. Ohtsubo, M. Iwakuma, S. Sato, K. Sakaki, A. Tomioka, T. Miyayama, M. Konno, H. Hayashi, H. Okamoto, Y. Gosho, T. Eguchi, T. Saitoh, T. Izumi, and Y. Shiohara. "Development of REBCO superconducting transformers with a current limiting function—Fabrication and tests of 6.9 kV-400 kVA transformers," IEEE Transactions on Applied Superconductivity, vol. 25, no. 3, pp. 1-5, 2014.
- [18] D. Hu, Z. Li, Z. Hong, and Z. Jin. "Development of a single-phase 330kVA HTS transformer using GdBCO tapes," Physica C: Superconductivity and its applications, vol. 539, pp. 8-12, 2017.
- [19] S. Hellmann, M. Abplanalp, S. Elschner, A. Kudymow, and M. Noe, "Current Limitation Experiments on a 1 MVA-Class Superconducting Current Limiting Transformer," IEEE Transactions on Applied Superconductivity, vol. 29, no. 5, Art. no. 5501706, 2019.
- [20] W. Song, Z. Jiang, M. Staines, R. A. Badcock, and J. Fang, "Experimental and numerical transport AC losses in a four-strand Roebel cable bifilar stack," *Superconductor Science and Technology*, vol. 31, Art. no. 115001, 2018.
- [21] W. Goldacker, F. Grilli, E. Pardo, A. Kario, S. I. Schlachter, and M. Vojenčiak, "Roebel cables from REBCO coated conductors: a one-century-old concept for the superconductivity of the future," *Superconductor Science and Technology*, vol. 27, no. 9, Art. no. 093001, 2014.
- [22] N. J. Long, R. A. Badcock, K. Hamilton, A. Wright, Z. Jiang, and L. S. Lakshmi, "Development of YBCO Roebel cables for high current transport and low AC loss applications," *Journal of Physics: Conference Series*, vol. 234, no. 2, Art. no. 022021, 2010.
- [23] S. S. Fetisov, V. V. Zubko, S. Y. Zanegin, et al., "Development and characterization of a 2G HTS Roebel cable for aircraft power systems," *IEEE Transaction on Applied Superconductivity*, vol. 26, no. 3, Art. no. 4803204, Apl. 2016.
- [24] Z. Jiang, M. Staines, N. J. Long, et al, "The scaling of transport AC losses in Roebel cables with varying strand parameters," *Superconductor Science and Technology*, vol. 27, no. 7, Art. no. 075007, 2014.
- [25] W. Song, Z. Jiang, X. Zhang, M. Staines, R. Badcock, J. Fang, Y. Sogabe, and N. Amemiya, "AC loss simulation in a HTS 3-Phase 1 MVA transformer using H formulation," *Cryogenics*, vol. 94, pp. 14-21, 2018.
- [26] Z. Hong, A. M. Campbell, and T. A. Coombs, "Numerical solution of critical state in superconductivity by finite element software," *Superconductor Science and Technology*, vol. 19, pp. 1246–1252, 2006.
- [27] R. Brambilla, F. Grilli, and L. Martini, "Development of an edge-element model for AC loss computation of high-temperature superconductors," *Superconductor Science and Technology*, vol. 20, pp. 16–24, Nov. 2006.
- [28] V. M. R. Zermeno, N. Mijatovic, C. Træholt, T. Zirngibl, E. Seiler, A. B. Abrahamsen, N. F. Pedersen, and M. P. Sorensen, "Towards faster FEM simulation of thin film superconductors: a multiscale approach," *IEEE Transaction on Applied Superconductivity*, vol. 21, pp. 3273–3276, 2011.
- [29] M. Zhang, J. H. Kim, S. Pamidi, M. Chudy, W. Yuan, and T. A. Coombs, "Study of second generation, high-temperature superconducting coils: Determination of critical current," *Journal of Applied Physics*, vol. 111, no. 8, Art. no. 083902, 2012.
- [30] V. M. Zermeno, A. B. Abrahamsen, N. Mijatovic, B. B. Jensen, and M. P. Sørensen, "Calculation of alternating current losses in stacks and coils made of second generation high temperature superconducting tapes for large scale applications," *Journal of Applied Physics*, vol. 114, Art. no. 173901, 2013.
- [31] Y. Kim, C. F. Hempstead, and A. R. Strnad, "Critical persistent currents in hard superconductors," *Physics Review Letter*, vol. 9, pp. 306–309, 1962.
- [32] E. Pardo, J. Šouc, and J. Kováč, "AC loss in ReBCO pancake coils and stacks of them: modelling and measurement," Superconductor Science and Technology, vol. 25, no. 3, Art. no. 035003, 2012.
- [33] Z. Jiang, N. J. Long, M. Staines, Q. Li, R. A. Slade, N. Amemiya, and A. D. Caplin, "Transport AC loss measurements in single- and two- layer parallel coated conductor arrays with low turn numbers," *IEEE Transaction on Applied Superconductivity*, vol.22, no. 6, Art. no. 8200306, 2012.

- [34] M. Staines and Z. Jiang, "Measurement of AC loss in individual turns of an HTS solenoid," *Physics Procedia*, vol.36, pp. 859-865, 2012.
- [35] Z. Jiang, R. A. Badcock, N. J. Long, et al., "Transport AC loss characteristics of a nine strand YBCO Roebel cable," Superconductor Science and Technology, vol. 23, Art. no. 025028, 2010.
- [36] https://www.mag-inc.com/Media/Magnetics/Datasheets/C058907A2.pdf.
- [37] J. K. Sykulski, K. F. Goddard, and R. L. Stoll, "A method of estimating the total AC loss in a high-temperature superconducting transformer winding," *IEEE Transactions on Magnetics*, vol. 36, no. 4, pp. 1183-1187, 2000.
- [38] E. Pardo, J. Šouc, and M. Vojenčiak, "AC loss measurement and simulation of a coated conductor pancake coil with ferromagnetic parts," *Superconductor Science and Technology*, vol. 22, no. 7, Art. No. 075007, 2009.
- [39] F. Herzog, T. Kutz, M. Stemmle, and T. Kugel, "Cooling unit for the AmpaCity project One year successful operation", *Cryogenics*, vol. 80, no. 2, pp. 204-209, 2016.
- [40] M. Yazdani-Asrami, M. Staines, G. Sidorov, et al., "Fault current limiting HTS transformer with extended fault withstand time", *Superconductor Science and Technology*, vol. 32, Art. no. 035006, 2019.

Correspondent author. E-mail: zhenan.jiang@vuw.ac.nz